Journal of
Mechanics of
Materials and Structures

APPLICATION OF A LUMPED DISSIPATION MODEL TO REINFORCED CONCRETE STRUCTURES WITH THE CONSIDERATION OF RESIDUAL STRAINS AND CYCLES OF HYSTERESIS

Francisco Adriano de Araújo and Sergio Persival Baroncini Proença

Volume 3, Nº 5 May 2008

mathematical sciences publishers

JOURNAL OF MECHANICS OF MATERIALS AND STRUCTURES
Vol. 3, No. 5, 2008

APPLICATION OF A LUMPED DISSIPATION MODEL TO REINFORCED CONCRETE STRUCTURES WITH THE CONSIDERATION OF RESIDUAL STRAINS AND CYCLES OF HYSTERESIS

FRANCISCO ADRIANO DE ARAÚJO AND SERGIO PERSIVAL BARONCINI PROENÇA

The nonlinear analysis model for reinforced concrete plane frame structures is based on the simplified concept of the localization of irreversible physical processes at previously definite zones, denominated here as generalized hinges. However, when both damage due to the microcracking of concrete and sliding mechanisms (aggregate interlocking) at crack surfaces are taken into consideration, hysteresis loops can be reproduced if the loading history includes unloading cycles. The thermodynamic approach of the model is herein developed with reference to generalized variables due to its application in the framework of the classical theory of bars under bending load. According to this model, there are three scalar variables: a damage variable, the plastic rotation of the section and the sliding-associated rotation of the section. By comparison with available experimental responses, the numerical examples illustrate the good performance of the model.

1. Introduction

As a natural progress of the constitutive modeling of materials coupling different phenomena such as elasticity, plasticity and microcracking, the Continuous Damage Mechanics has been efficiently applied since the early eighties. Some of the resulting models encompassing complex responses are nowadays greatly diffused. Among the coupled phenomena considered, one can mention creep damage [Murakami 1981; Kachanov 1984], fatigue damage [Marigo 1985], creep-damage-fatigue interaction [Lemaitre and Chaboche 1974], ductile damage [Simo and Ju 1987; Tai 1990], reinforced concrete damage [Mazars 1984], reinforced and fiber concrete under seismic response [La Borderie et al. 1991].

Concerning reinforced concrete modeling, most of the subsequent publications have, as a common ground, the high level of complexity in terms of formulation and required discretization especially on what concerns numerical analysis. However, when their application to framed structures is considered, such complexities increase the computational costs and imply loss in efficiency. Hence, despite consideration of coupled phenomena, the so-called simplified models were explored as a more adequate alternative. Pioneering works in this direction include [Riva and Cohn 1990a; 1990b; Mulas and Filippou 1990; Alves and Lubliner 1992; Flórez-López 1993].

A common feature of the simplified models is to assume that the material nonlinear response related phenomena are lumped in zones of energy dissipation. Actually, this concept was originally proposed in lumped plasticity models [Maier et al. 1973; Cohn and Franchi 1979; Riva and Cohn 1990a; 1990b].

Keywords: damage mechanics, plastic hinge, hysteresis.

With the major focus on reinforced concrete framed structures, the Flórez-López simplified model presumes that the damage and plasticity evolutive processes are localized at regions of length zero denominated as generalized hinges. The formulation adopted is based on the thermodynamics of solids and accounts for the appearance of permanent strains and stiffness reduction in elements submitted to monotonic loading or reversible loading without sign inversion.

On the other hand, still within the framework of the complex constitutive modeling, the subject of the damping of structural dynamic response resulting from microcracking evolutive processes in the material was originally treated in [Mazars et al. 2000] by employing Continuous Damage Mechanics. The reproduction of hysteretic loops observed experimentally in uniaxial stress-strain diagrams of concrete under unloading and reloading cycles was the most basic issue considered. Based on the aforementioned, two dissipative phenomena present in concrete are considered: diffuse microcrack growth (damage) and the sliding tendency combined with aggregate interlocking between microcracks faces.

The formulation of the Marzar model is also based on the framework of the thermodynamics of solids. Accordingly, the phenomena to be modeled can be represented by two internal state variables: a scalar damage variable and a sliding strain variable. Hence, in order to derive the constitutive model, a thermodynamic potential representing the free energy at a certain state and a dissipative potential are defined. From the free energy potential one can derive the well-known associated variables while from the dissipative potential, one derives the evolution laws for the internal state variables.

With the major aim being the analysis of plane reinforced concrete framed structures, the present work proposes the insertion of Mazars' formulation in the scope of the simplified model formulated originally by Flórez-López [1993] and in such way that the same phenomena described in the complex model remain considered. However, since generalized stress (bending moment) and strain variables (rotation) are now involved, the internal variable related to the sliding effect is defined as a sliding rotation. A major hypothesis considered is an ideal bonding between concrete and steel bars, since debonding could affect hysteresis loops.

Essentially, three new elements are then introduced: the possibility of occurrence of residual strains due to concrete as well as steel behavior (in the original model only the plastic flow of steel is considered), the employment of an alternative damage criterion function and the introduction of a sliding-associated rotation variable ϕ_s (invoked from the hysteresis loops).

2. Thermodynamic framework of the model

Since this is a model for framed plane structures, in which the dissipative processes are located in zones of null dimensions, the structures are admitted to be formed by bar elements with the possibility of forming hinges at their ends. Away from the hinged zones, the elements remain in elastic regime as shown in Figure 1.

The total hinge rotations result from the effect of different phenomena: elastic strain, damage and plasticity of concrete, steel plasticity and sliding between microcrack faces. In the present idealized model, it is considered that the latter effect is manifested in parallel with the other phenomena and can be represented separately as illustrated in Figure 2. The figure compares the initial (a) and deformed (b) configurations of the ends of an element according to bending theory (plane sections, shear strain disregarded).

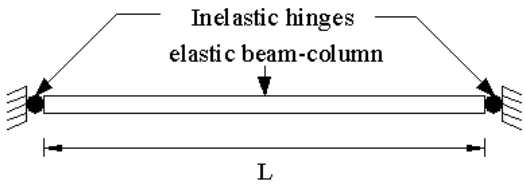

Figure 1. Bar element of the lumped dissipation models.

The nomenclature indicated in Figure 2 has the following meaning:

- k_e is the beam-column elastic stiffness;
- $k_d(d)$ is the portion of hinge stiffness associated to damage;
- $k_s(d)$ is the hinge stiffness associated to slip;
- ϕ is the total hinge rotation;
- ϕ_e is the portion of rotation resulting from elastic deformation of the beam;
- ϕ_d is the portion of hinge rotation due to damage;
- ϕ_p is the portion of rotation due to plastification (concrete and steel) at hinge;
- ϕ_s is the rotation due to slip (it represents the sliding between the concrete fracture surfaces).

In correspondence to the various terms of rotation: rotation due to damage, rotation due to plastification and rotation due to sliding, the moment at the element edge is divided into terms of denominated moment: moment due to damage, moment due to plastification and, in another term, moment due to slip, which is also dependent on the level of damage of the structure. The bending due to slip is related to the sliding-associated rotation which can develop during both the loading process and the reloading and

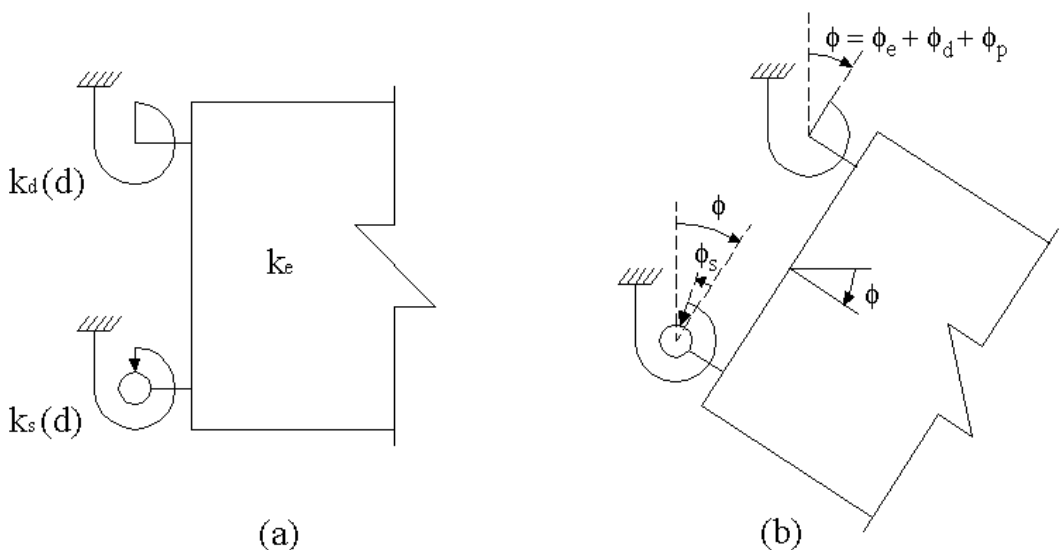

Figure 2. Physical representation of hinge stiffness and rotations: (a) initial configuration; (b) deformed configuration.

unloading cycles. Plastification, which develops from only loading processes, does not however show this characteristic.

Three criteria are hence introduced to control the evolution of the model variables: the damage criterion which identifies the possibility of evolution of the damage variable, the plastification criterion which indicates the possibility of evolution of plastic rotation, and the slip criterion which accuses the possibility of evolution of any slip rotation. It is worth observing that since slip is associated to movement between microcrack surfaces and the latter in turn translate in damage, slip rotation will only occur with the occurrence of damage.

The formulation of the model follows a thermodynamics-based approach applied to solids [Lemaitre and Chaboche 1985], such that the model variables and the corresponding evolution laws maintain coherence with the principles of thermodynamics.

Consider therefore a typical bar element with end hinges as shown in Figure 3. The same figure presents the positive conventions for degrees of freedom of interest (axial strains are not considered).

The scalar damage variable and the representative variables (vectorial) of the portion of rotation and the strain hardening can together be denominated as internal state variables. The existence of a certain amount of energy claimed to be free, or that can be made available for accomplishing work from a current element state is assumed.

As usual, the damage is supposed to directly affect the initial rigidity of the material. On the other hand, in order to account for aggregate interlocking, a plasticity-based approach is used to model the sliding effect. However, since a certain level of coupling is supposed to exist between the internal state variables, the damage variable appears also multiplying the sliding term in the free energy. As a consequence, in the model, sliding occurs only after the appearance of damage, which is physically consistent.

Therefore, adopting the Helmholtz specific free energy as the free energy potential and admitting that the bar element, in its current state, presents a certain level of damage, plastic rotation and slip rotation (with a certain associated strain hardening level), we propose the potential

$$\chi = \chi_{dp} + \chi_s \,,$$

where $\chi_{dp} = \frac{1}{2}(\phi - \phi_p)^T \underline{K_{ed}(d)}\,(\phi - \phi_p)$, $\chi_s = \frac{1}{2}(\phi - \phi_s)^T \underline{K_s(d)}\,(\phi - \phi_s) + \frac{1}{2}\,b\,\alpha^T\alpha$, and

- χ is the total free energy potential;
- χ_{dp} is the portion of free energy after deducing the effects of damage and the plastification;
- χ_s is the portion of free energy associated to the slip process and strain hardening between microcrack faces;

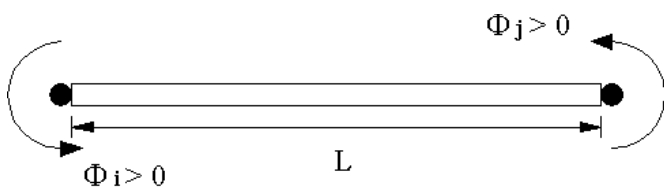

Figure 3. Bar element under study and positive convention for end rotations.

- $\phi = \binom{\phi_i}{\phi_j}$ is the vector of total rotations at the i-th and j-th ends of the element;
- $\phi_p = \binom{\phi_{pi}}{\phi_{pj}}$ is the vector of plastic rotations at the element extremities;
- $\phi_s = \binom{\phi_{si}}{\phi_{sj}}$ is the vector of slip rotations at the element extremities;
- $\alpha = \binom{\alpha_i}{\alpha_j}$ is the vector of the strain hardening variable associated to components of slip rotation;
- b is a material parameter;
- $\underline{K_{ed}(d)}$ is the element elastic-damage stiffness matrix;
- $\underline{K_s(d)}$ is the element slip stiffness matrix.

For the elasto-damaged stiffness matrix we adopt an expression similar to that presented by Flórez-López [1993]. Such a matrix is made up of contributions of the beam-column elastic stiffness and the hinge damage stiffness:

$$\underline{K_{ed}(d)} = \begin{pmatrix} \dfrac{(1-d_i)(4-d_j)}{4-d_i d_j}\dfrac{4EI}{L} & \dfrac{4(1-d_i)(1-d_j)}{4-d_i d_j}\dfrac{2EI}{L} \\ \dfrac{4(1-d_i)(1-d_j)}{4-d_i d_j}\dfrac{2EI}{L} & \dfrac{(1-d_j)(4-d_i)}{4-d_i d_j}\dfrac{4EI}{L} \end{pmatrix},$$

where

- d_i, d_j are variables that quantify the damage suffered by the hinge at extremities i and j respectively;
- $E = \frac{E_c(A_c - A_s) + E_s A_s}{A_c}$ is the homogenized modulus of elasticity; with E_c, E_s the Young's moduli of concrete and steel respectively, and A_c, A_s the concrete cross section and the total steel reinforcement areas respectively;
- I is the moment of inertia of complete bar transversal section;
- L is the element length.

Invoking the components of the main diagonal of the stiffness matrix of the element in a pure elastic state, we postulate the part of stiffness due to slip effect between microcrack faces in the present work to take the form

$$\underline{K_s(d)} = \frac{4EI}{L}\begin{pmatrix} d_i & 0 \\ 0 & d_j \end{pmatrix}. \tag{2-1}$$

The introduction of the damage level in each hinge in the slip stiffness matrix is intentional with the aim of reproducing the coupling between damage and slip, more specifically, the dependence of the latter in relation to the former. Actually, experimental observations justify the fact that every inelastic phenomenon of concrete is manifested from the appearance and evolution of microcracks [Ragueneau et al. 2000]. In addition, the diagonal structure of the slip matrix implies that no coupling is assumed between hinges.

The thermodynamic admissibility of the model is guaranteed by imposing the Clausius–Duhem inequality which implies that dissipation of the deformation process cannot be negative. Considering that in the case of the classical bending theory, strain results from the effects of bending moments and ignoring

any other nonmechanical effect such as thermal effects, we can write the relation expressing the evolution of dissipation as

$$M \cdot \dot{\phi} - \dot{\chi} \geq 0. \tag{2-2}$$

In the previous relation, the first term is the *rate* (the time variation, to better represent an evolutive process) of internal energy involved in the bending process. The dot on the variable represents the derivative of the variable with respect to time.

Assume the thermodynamic potential can be linearized in the neighbourhood of current values of the state variables. Then it follows that

$$\dot{\chi} = \frac{\partial \chi}{\partial \phi} \cdot \dot{\phi} + \frac{\partial \chi}{\partial \phi_p} \cdot \dot{\phi}_p + \frac{\partial \chi}{\partial \phi_s} \cdot \dot{\phi}_s + \frac{\partial \chi}{\partial d} \cdot \dot{d} + \frac{\partial \chi}{\partial \alpha} \cdot \dot{\alpha}.$$

The linearized potential can now be substituted in (2-2) thus resulting in

$$\left(M - \frac{\partial \chi}{\partial \phi}\right) \cdot \dot{\phi} - \frac{\partial \chi}{\partial \phi_p} \cdot \dot{\phi}_p - \frac{\partial \chi}{\partial \phi_s} \cdot \dot{\phi}_s - \frac{\partial \chi}{\partial d} \cdot \dot{d} - \frac{\partial \chi}{\partial \alpha} \cdot \dot{\alpha} \geq 0. \tag{2-3}$$

The last inequality must be valid for any process including a purely reversible process where

$$\dot{\phi}_p = \dot{\phi}_s = \dot{d} = \dot{\alpha} = 0.$$

One way to ensure that this process is included in inequality (2-3) consists of imposing the following condition now expressed in matrix notation:

$$M = \frac{\partial \chi}{\partial \phi} = \underline{K_{ed}(d)}(\phi - \phi_P) + \underline{K_s(d)}(\phi - \phi_s), \tag{2-4}$$

which defines M as the thermodynamic variable associated with ϕ. By analogy, thermodynamic variables associated to the other state variables can be defined

$$M_{dp} = \frac{\partial \chi}{\partial \phi_p} = -\underline{K_{ed}(d)}(\phi - \phi_p)\,, \tag{2-5}$$

$$M_s = \frac{\partial \chi}{\partial \phi_s} = -\underline{K_s(d)}(\phi - \phi_s)\,, \tag{2-6}$$

$$Y = \frac{\partial \chi}{\partial d} = \frac{1}{2}\frac{\partial}{\partial d}\left((\phi - \phi_p)^T \underline{K_{ed}(d)}(\phi - \phi_p)\right) + \frac{1}{2}\frac{\partial}{\partial d}\left((\phi - \phi_s)^T \underline{K_s(d)}(\phi - \phi_s)\right), \tag{2-7}$$

$$X = \frac{\partial \chi}{\partial \alpha} = b\alpha. \tag{2-8}$$

Thus M_{dp}, M_s, Y and X are the thermodynamic variables associated to respectively, the state variables ϕ_p, ϕ_s, d and α. In particular, still, due to the fact that the modelling of strain hardening will be based on its analogy with plasticity, the variable X will here be denominated as the kinematic strain hardening moment.

What can easily be observed from (2-4), (2-5) and (2-6) is that the resulting total moment at the extremities of the element consists of two parts: one involving the elastic rigidity penalized by the damage (M_{dp}) and the other involving an additional rigidity related to the aggregate interlocking effect (M_s). In particular, this term is also dependent on the damage level in such way that the expected stiffening effect is reproduced. Moreover, it is also important to note that (2-6) defining the associated

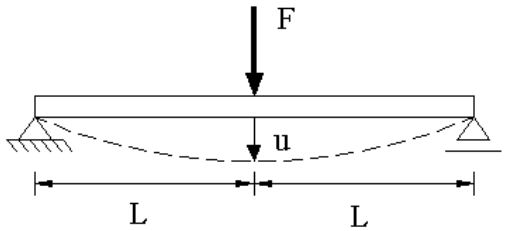

Figure 4. Bending test scheme.

sliding moment includes a rotation term. This term reduces when the sliding rotation increases thus reducing the moment even if the damage attains unit value. What happens finally is that the hysteresis loops and resulting irreversible strains given by the model are enlarged as the damage increases, which is consistent with the experimental responses as the one illustrated in Figure 5.

Moreover, considering (2-3) and equations (2-4)–(2-8), we conclude that the dissipated energy is nonnegative provided the following condition is satisfied:

$$M_{dp} \cdot \dot{\phi}_p + M_s \cdot \dot{\phi}_s - Y \cdot \dot{d} - X \cdot \dot{\alpha} \geq 0.$$

Relative to those portions that are dependent on the effects of slip, it can be shown that positive dissipation is automatically verified so long as the evolution laws of the internal variable associated to this phenomenon (ϕ_s and α) are derived from a convex dissipation potential [Ragueneau et al. 2000] (this aspect will be reviewed in the next section). In order to ensure that $-Y \cdot \dot{d} \geq 0$ for the modeling in the present work, the damage criterion proposed by Alva [2004] is invoked from experimental results.

3. Damage, plasticity and flow criteria

Consider the structural system illustrated in Figure 4 in terms of generalized variables. The system response can be evaluated by the midsection bending moment versus midsection rotation diagram as illustrated in Figure 5.

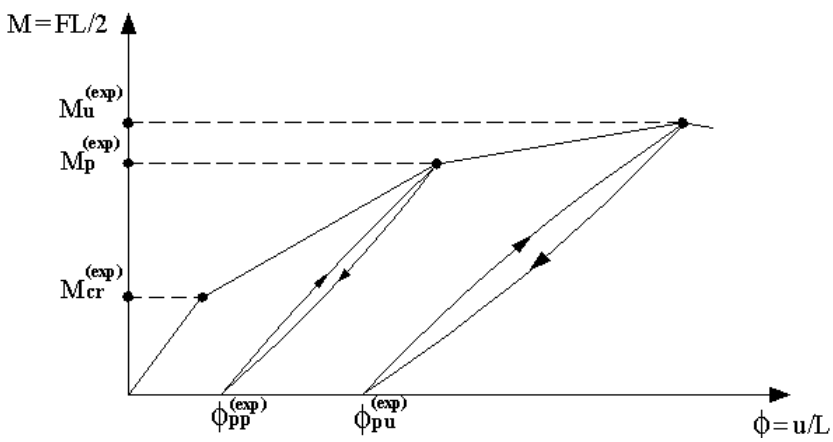

Figure 5. The mid-span moment-rotation experimental diagram.

In Figure 5 the following characteristic parameters are highlighted:

- $M_{cr}^{(\exp)}$ is the critical moment at the beginning of damage of concrete;
- $M_{p}^{(\exp)}$ is the moment corresponding to the beginning of plastification of steel;
- $M_{u}^{(\exp)}$ is the peak moment corresponding to the maximum strength of the section;
- $\phi_{pp}^{(\exp)}$ is the residual rotation due to damage of concrete at the start of steel plastification;
- $\phi_{pu}^{(\exp)}$ is the plastic (peak) rotation corresponding to the peak moment.

These parameters can be determined experimentally by carrying out the experimental test schematized in Figure 4.

As already mentioned, the total moment at the extremities of the element is composed of two distinct parts ($M = M_{dp} + M_s$). Figure 11, placed much further in the text for convenience, illustrates these parts. It is worth remembering that only bending moments at the element extremity i are considered. The part M_{dp} is associated to damage and plasticity of concrete and steel. This portion is used directly in the criteria that define the start and evolution of damage and plasticity in hinges.

For those functions, the proposal in [Alva 2004] and an adaptation of the expression presented by Flórez-López [1998] are respectively adopted. These criteria are given by

$$g = G - G_{cr} - \theta \frac{q \ln(1-d)}{1-d} \leq 0\,, \tag{3-1a}$$

$$f = \left| \frac{M_{dp}}{1-d} - c\phi_p \right| - M_{cr} \leq 0, \tag{3-1b}$$

where

$$G = \frac{1}{2S_0}\left(\frac{M_{dp}}{1-d}\right)^2, \qquad G_{cr} = \frac{{M_{cr}}^2}{2S_0}, \qquad \theta = \exp(-\gamma(1-d)),$$

with $S_0 = \frac{4EI}{L}$, d is the damage at the extremity of the element, M_{dp} is the operating moment, ϕ_p is the plastic rotation, γ is a parameter to be determined from the experimental response of the element, c and q are additional parameters to be determined indirectly.

It is worth remembering again that in hinges the previous functions are associated exclusively to the damage and plastification processes. Therefore, the parameter M_{cr} introduced in (3-1b) is not exactly equal to $M_{cr}^{(\exp)}$ shown in Figure 5. With the aim of employing the experimental values $M_{cr}^{(\exp)}$, $M_{p}^{(\exp)}$, $M_{u}^{(\exp)}$ in the parametric identification, it is considered that M_{cr} is related to $M_{cr}^{(\exp)}$ through the penalty factor η whose value depends on the average width of the hysteresis loops. The same proposal is extended to other model parameters of interest. Therefore, the penalization in question takes the following set of relations:

$$\begin{cases} M_{cr} = \eta \cdot M_{cr}^{(\exp)}, \\ M_{p} = \eta \cdot M_{p}^{(\exp)}, \\ M_{u} = \eta \cdot M_{u}^{(\exp)}. \end{cases} \tag{3-2}$$

It is worth saying before hand that the value $\eta = 0.9$ was the most representative value for the examples considered in this work. In Figure 6, an interpretation for the relations in (3-2) is given.

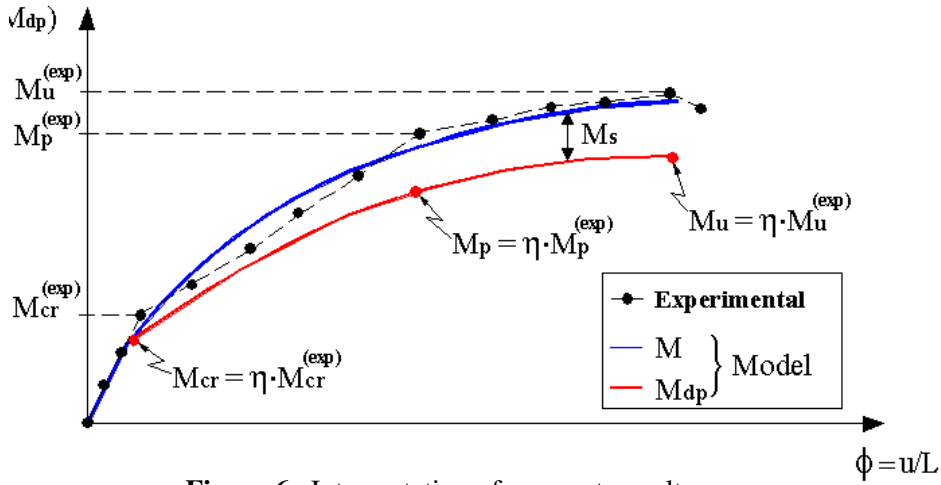

Figure 6. Interpretation of moment penalty.

Expression (3-1a), originally presented by Alva [2004], introduces a new parameter γ, in the definition for θ, that needs to be identified from experimental tests on the damage of the hinge. Along this direction, as a first step, the evolution law that governs the damage d appearing in the relation θ must be identified from successive values of stiffness corresponding to the slopes of the unloading curves as illustrated in Figure 7. These stiffness values also serve for constructing the experimental response curve which relates the damage to the thermodynamic moment G (assuming $M_{dp} = M$). In the following step, the value of γ is obtained from best fit between the experimental and the numerically obtained curves which represent the damage versus thermodynamic moment G relation; see Figure 8.

In order to consider the processes of plastification of concrete and the steel-concrete, the behavior described in Figure 9 is proposed to the parameter c, which appears in (3-1b). Basically, there are two groups of values, c_p and c_u, corresponding to the already cited plastification. A transition between the two groups of values is also assumed in order to prevent numerical problems.

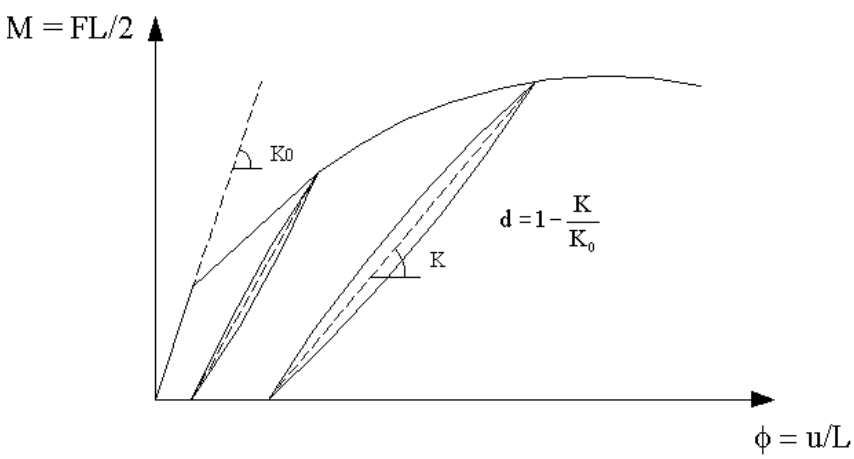

Figure 7. Determination of the experimental values of the damage.

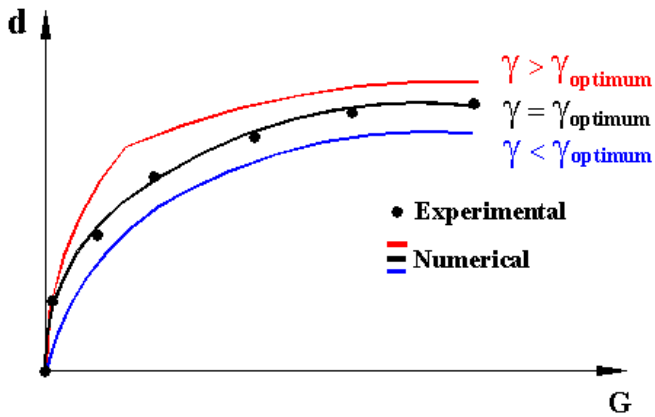

Figure 8. Calibration of the variable γ.

Note that the bending moment M_y is used as reference for the transition part between the values of c. In the present work, the relation

$$M_y = \frac{3M_p + M_u}{4},$$

which corresponds to dividing the interval (M_p, M_u) into four equally spaced subintervals, with M_y being one of the extremities of first subinterval, is adopted.

For the remaining parameters c_p, c_u and q, no well defined mechanical interpretation is given; simply speaking, the values of these parameters can be determined indirectly by imposing certain complementary conditions. On determining these values, two other reference parameters d_u and d_p are observed to appear. For example, the following conditions determine the constants q and d_u:

$$\begin{cases} g = 0,\ M_{dp} = M_u,\ d = d_u \Rightarrow (1-d_u)^2 G_{cr} + \theta_u q (1-d_u)\ln(1-d_u) - \dfrac{M_u^2}{2S_0} = 0, \\ g = 0,\ \dfrac{\partial (M_{dp}^2)}{\partial d} = 0,\ d = d_u \Rightarrow -2(1-d_u)G_{cr} - \theta_u q (h_u \ln(1-d_u) + 1) = 0, \end{cases} \tag{3-3}$$

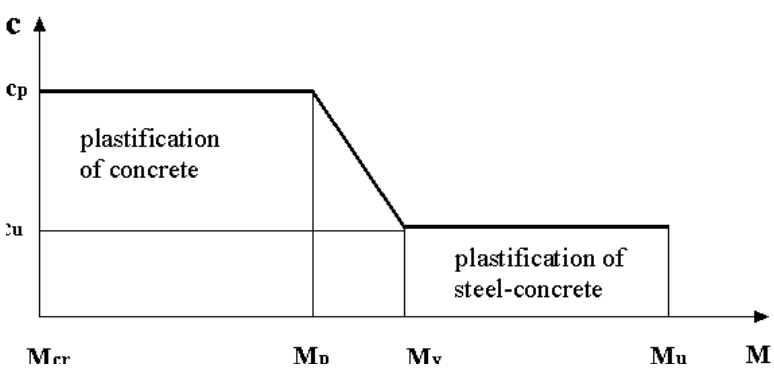

Figure 9. Behavior of parameter c.

where $\theta_u = \exp(-\gamma(1-d_u))$ and $h_u = 1+\gamma d_u - \gamma$. Respectively, the conditions in (3-3) impose that for the ultimate moment that verifies the criterion with the equality, a corresponding damage d_u exists and for this damage level there is a corresponding maximum for M_{dp}.

On the other hand the solution of the following equation provides the value for d_p:

$$g = 0,\ M_{dp} = M_p,\ d = d_p \Rightarrow \frac{{M_p}^2}{2(1-d_p)^2 S_0} - G_{cr} - \theta_p \frac{q\ln(1-d_p)}{1-d_p} = 0,$$

where $\theta_p = \exp(-\gamma(1-d_p))$ and d_p is the damage corresponding to the moment of plastification of steel reinforcement.

The constants c_p and c_u are obtained from the following equations

$$\begin{cases} f = 0,\ M_{dp} = M_p \Rightarrow c_p = \dfrac{1}{\phi_{pp}}\left(\dfrac{M_p}{1-d_p} - M_{cr}\right), \\ f = 0,\ M_{dp} = M_u \Rightarrow c_u = \dfrac{1}{\phi_{pu}}\left(\dfrac{M_u}{1-d_u} - M_{cr}\right), \end{cases}$$

thus completing the process of obtaining all necessary damage and plastification parameters. Considering the criterion that defines the start and evolution of the rotation in hinges, which thus reflects the slip between the microcrack surfaces, we propose the following form:

$$f_s = |M_s - X| - M_k \le 0, \tag{3-4}$$

where the constant M_k is large enough to prevent numerical problems, but still very small such that the evolution of slip occurs nearly simultaneously with the evolution of damage. Figure 10 includes a representation of relation (3-4).

The inequality (3-4) applies to the loading, unloading and reloading stages. As it will be seen later in the solution strategy, violation of the condition $f_s \le 0$ will serve to characterize, for the loading step under consideration, whether or not the slip process evolves, the degree of resistance to its evolution being represented at a minor or major scale by the value of X.

With relation to the evolution laws of the slip associated internal variables expressed by $\dot{\phi}_s$ and $\dot{\alpha}$, a procedure analogous to that used in the nonassociative plasticity theory is adopted. Therefore the dissipative energy is employed with essentially similar expressions to those of the slip criterion. However, in order

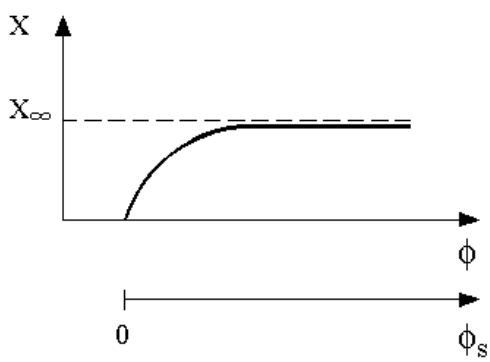

Figure 10. The kinematic nonlinear strain hardening moment.

to introduce the possibility of describing nonlinear strain hardening, the following form is considered for the dissipative potential:

$$\psi_s = |M_s - X| + \tfrac{3}{4}aX^2 - M_k, \tag{3-5}$$

where a is a material parameter. The term $\frac{3}{4}aX^2$ is responsible for strain hardening nonlinearity and for the tendency to reach an asymptotic value as it will be shown afterwards.

Hence, imposing the normality rule on the surface of the dissipative potential, we can give the evolution laws for the internal variables as

$$\dot{\phi}_s = \dot{\lambda}\frac{\partial \psi_s}{\partial M_s}, \tag{3-6a}$$

$$\dot{\alpha} = -\dot{\lambda}\frac{\partial \psi_s}{\partial X}, \tag{3-6b}$$

where $\dot{\lambda}$ maintains the similarity with the plastic multiplier of plasticity and the negative sign of the expression of $\dot{\alpha}$ guarantees positive dissipation.

A condition introduced in the model is that the kinematic strain hardening moment, now nonlinear, tends to an asymptotic value X_∞ as the values of rotation become higher since under such a situation the slip between microcrack faces ceases to increase.

To obtain this limit value, (2-8) is considered thus leading to

$$\dot{X} = b\dot{\alpha}. \tag{3-7}$$

From a combination of expression (3-7), (3-6b) and (3-5), we have

$$\dot{X} = b\dot{\lambda}(\operatorname{sign}(M_s - X) - \tfrac{3}{2}aX). \tag{3-8}$$

Admit $\operatorname{sign}(M_s - X) = 1$. Therefore, $\lim_{\frac{3}{2}aX \to 1} \dot{X} = 0$. Therefore, the limit value for X can be obtained when the equality

$$X_\infty = \frac{2}{3a}$$

is true. The curve presented in Figure 10 is obtained from the numerical integration of expression (3-8).

Finally, the meaning of each terms of the moments considered in this model are shown in Figure 11.

The hysteresis loop is here characterized by the noncoincidence of the curves defined in the unloading and reloading stages in the moment-rotation diagram. The model under analysis is aimed at generating hysteresis loops of unloading and reloading cycles as shown in Figure 12.

Figure 12 (a) is a representation of the contribution of various rotation terms ϕ_e, ϕ_p, ϕ_d that make up the total rotation $\phi = \phi_e + \phi_p + \phi_d$ for the load level corresponding to point B.

4. Implementation of the model

The model was implemented using a special proposed nonlinear analysis plane frame software. The main strategy employed was the Newton–Raphson incremental-iterative method with a step-by-step load application followed by successive corrections of equilibrium [Ortiz and Simo 1986]. The integration of the constitutive model including a determination of the damage variable, plastic rotation, slip rotation and the variable associated to the kinematic nonlinear strain hardening of the hinges at each iteration follows an iterative approach.

The damage evolution in each hinge is obtained by imposing nullity condition on the damage criterion (3-1a) since this criterion must have already been violated in the i-th ($g^{(i)} > 0$) iteration step. Therefore, for the $(i+1)$-th iteration we have

$$\Delta d^{(i+1)} = \frac{-g^{(i)}}{\frac{\partial g}{\partial d}\Big|^{(i)}} = \frac{g^{(i)}}{\left(\theta_q\left(\frac{\ln(1-d)-1}{(1-d)^2}\right) + \gamma\theta_q\left(\frac{\ln(1-d)}{1-d}\right) + \frac{2G}{1-d}\right)\Big|^{(i)}}.$$

Having updated the damage $d^{(i+1)} = d^{(i)} + \Delta d^{(i+1)}$, we verify the damage criterion again, with the successive update of damage until the criterion $g \leq 0$ is verified.

The evolution of plastic rotation of each hinge is also obtained by imposing the nullity condition on the plasticity criterion (3-1b) since this criterion must have been violated in i-th iteration ($f^{(i)} > 0$). Therefore, for the $(i+1)$-th iteration we have

$$\Delta\phi_p{}^{(i+1)} = \frac{-f^{(i)}}{\frac{\partial f}{\partial \phi_p}\Big|^{(i)}} = \frac{f^{(i)}}{(\text{sign}(\lambda)c)|^{(i)}},$$

where

$$\lambda = \frac{M}{1-d} - c\phi_p, \qquad \text{sign}(\lambda) = \begin{cases} +1 & \text{if } \lambda > 0, \\ -1 & \text{if } \lambda < 0. \end{cases}$$

After updating the plastic rotation $\phi_p{}^{(i+1)} = \phi_p{}^{(i)} + \Delta\phi_p{}^{(i+1)}$, the plasticity criterion is again verified. The successive updating of rotation is continued until the criterion $f \leq 0$ is verified.

Relative to the plastic multiplier, considering a hinge j of the finite element, as illustrated in Figure 3, we linearize the representative surface of the sliding criterion $f_s = 0$ using current values of the state variables in the i-th iteration of the same i-th step:

$$f_s{}^{(i+1)} = f_s{}^{(i)} + \frac{\partial f_s}{\partial M_s}\Big|^{(i)}\left(M_s{}^{(i+1)} - M_s{}^{(i)}\right) + \frac{\partial f_s}{\partial X}\Big|^{(i)}\left(X^{(i+1)} - X^{(i)}\right) = 0. \tag{4-1}$$

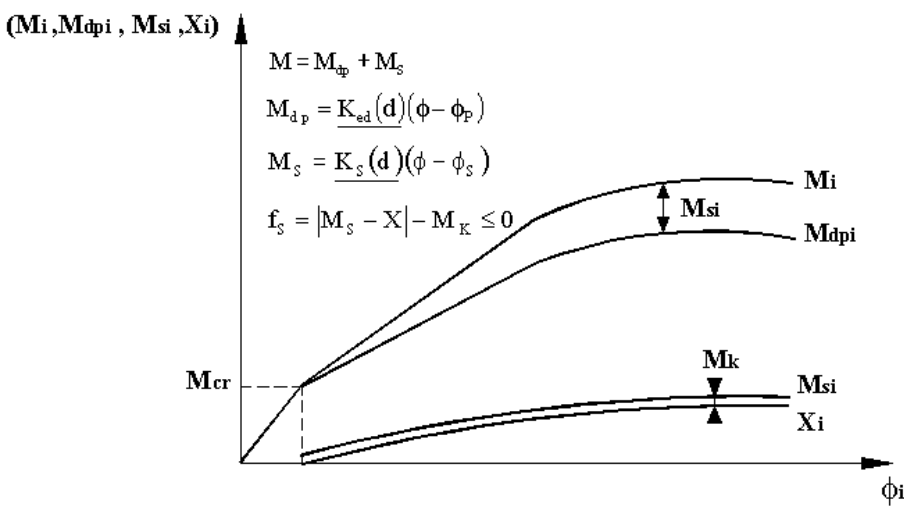

Figure 11. Various terms of the moments used in the model.

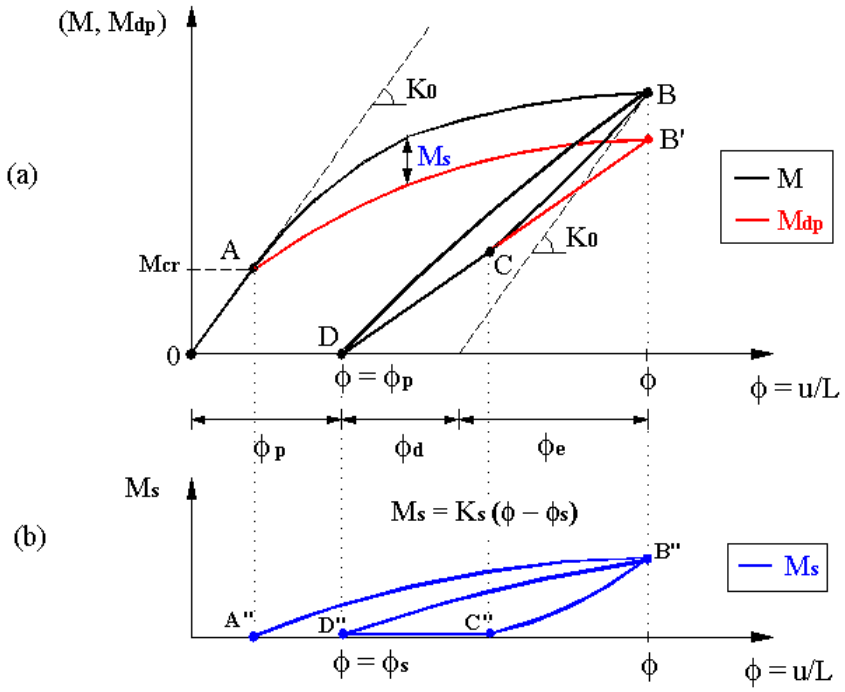

Figure 12. Hysteresis loop of (a) M, M_{dp} versus ϕ (b) M_s versus ϕ.

Knowing that for hinge j, in the i-th iteration we have

$$\dot{M}_s{}^{(i)} = -K_{s22}\dot{\phi}_s{}^{(i)} = -K_{s22}\Big(\dot{\lambda}\frac{\partial \psi_s}{\partial M_s}\Big)^{(i)}, \qquad \dot{X}^{(i)} = b\dot{\alpha}^{(i)} = -b\Big(\dot{\lambda}\frac{\partial \psi_s}{\partial X}\Big)^{(i)}. \tag{4-2}$$

By adopting an explicit relation such that

$$\dot{M}_s{}^{(i)}\Delta t = M_s{}^{(i+1)} - M_s{}^{(i)}, \qquad \dot{X}^{(i)}\Delta t = X^{(i+1)} - X^{(i)},$$

and substituting (4-2) in (4-1), we have

$$\Delta\lambda^{(i)} = \dot{\lambda}^{(i)}\Delta t = \frac{-f_s{}^{(i)}}{\frac{\partial f_s}{\partial M_s}\Big|^{(i)} K_{s22}\,\frac{\partial \psi_s}{\partial M_s}\Big|^{(i)} + \frac{\partial f_s}{\partial X}\Big|^{(i)} b\,\frac{\partial \psi_s}{\partial X}\Big|^{(i)}},$$

where K_{s22} is a component of the matrix given in (2-1). We have also

$$\frac{\partial f_s}{\partial M_s}\Big|^{(i)} = \operatorname{sign}\big(M_s{}^{(i)} - X^{(i)}\big), \qquad \frac{\partial \psi_s}{\partial M_s}\Big|^{(i)} = \operatorname{sign}\big(M_s{}^{(i)} - X^{(i)}\big),$$

$$\frac{\partial f_s}{\partial X}\Big|^{(i)} = -\operatorname{sign}\big(M_s{}^{(i)} - X^{(i)}\big), \qquad \frac{\partial \psi_s}{\partial X}\Big|^{(i)} = \operatorname{sign}\big(M_s{}^{(i)} - X^{(i)}\big) + \tfrac{3}{2}aX^{(i)},$$

where

$$a = \frac{2}{3X_\infty}, \quad \operatorname{sign}\big(M_s{}^{(i)} - X^{(i)}\big) = \begin{cases} +1 & \text{if } \big(M_s{}^{(i)} - X^{(i)}\big) > 0, \\ -1 & \text{if } \big(M_s{}^{(i)} - X^{(i)}\big) < 0. \end{cases}$$

Therefore once the slip criterion (3-4) is violated, the update of internal variables for the $(i+1)$-th iteration of the load step is carried out as shown in the following equations:

$$\phi_s{}^{(i+1)} = \phi_s{}^{(i)} + \Delta\lambda^{(i)} \frac{\partial \psi_s}{\partial M_s}\bigg|^{(i)}, \qquad X^{(i+1)} = X^{(i)} - \Delta\lambda^{(i)} b \frac{\partial \psi_s}{\partial X}\bigg|^{(i)}, \qquad M_s{}^{(i+1)} = K_{s22}\left(\phi - \phi_s{}^{(i+1)}\right).$$

Having obtained the new values, the slip criterion is again verified proceeding by successive updating until the criterion $f_s \le 0$ is verified. A similar procedure is applied to hinge i.

5. Strategy for considering the inversion of sign of the loading

In order to extend the model to include response under dynamic loading, it is necessary to determine the possibility of sign of the load being inverted. Based on this, the strategy proposed in [Flórez-López 1995] by defining two sets of independent variables, one associated to positive load and the other associated to negative loads according to the convention presented in Figure 13, is adopted.

Two scalar damage variables d^+ for $M > 0$ and d^- for $M < 0$, both with independent behaviors, are considered. However, for the plastic rotation ϕ_p, as well as for the slip rotation ϕ_s, only a single variable continues to exist. In each case there are the evolution laws that start to depend on the sign of the load. The damage, plastification and kinematic strain hardening criteria then assume a particular form depending on the sign of the loads. Thus, for positive load we have

$$g^+ = G^+ - G_{cr}^+ - \theta^+ \frac{q^+ \ln(1-d^+)}{1-d^+} \le 0, \qquad f^+ = \left| \frac{M_{dp}^+}{1-d^+} - \alpha c^+ \phi_p \right| - ((1-\alpha)c^+ p + M_{cr}^+) \le 0,$$
$$f_s^+ = |M_s^+ - X^+|\, M_k^+ \le 0,$$

while for negative load we have

$$g^- = G^- - G_{cr}^- - \theta^- \frac{q^- \ln(1-d^-)}{1-d^-} \le 0, \qquad f^- = \left| \frac{M_{dp}^-}{1-d^-} - \alpha c^- \phi_p \right| - ((1-\alpha)c^- p + M_{cr}^-) \le 0,$$
$$f_s^- = |M_s^- - X^-|\, M_k^- \le 0,$$

where $p = \max|\phi_p|$ and $0 \le \alpha \le 1$.

6. Examples of application

In order to evaluate the efficiency of the model under study, in the first example, results of experimental and numerical analyses for a beam presented in [Mazars et al. 2000] were compared. The cross section geometry and steel reinforcement is shown in Figure 14.

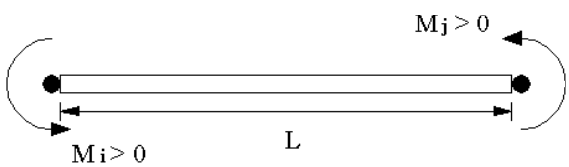

Figure 13. Positive convention for the nodal/end moments.

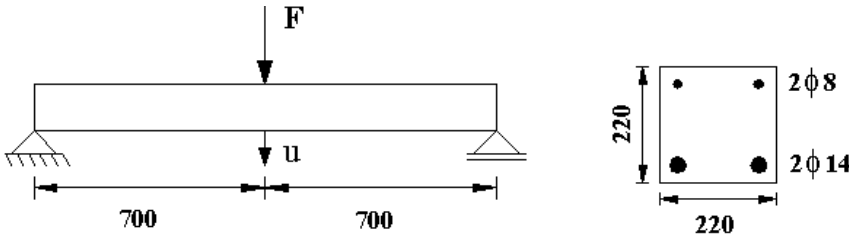

Figure 14. Geometry and beam reinforcement [Mazars et al. 2000].

In Figure 15, the numerical response is compared to the experimental response. Besides the numerical response obtained from the model under study, the response from another damage model [La Borderie et al. 1991] was also reproduced (in this model the damage is diffused in the element while the reinforcement bars are discretized into layers). The parameters of interest in the numerical modeling were calibrated based on the experimental result in [Ragueneau et al. 2000]. The values adopted are:

Properties of concrete:

$$E_C = 28000\,\text{MPa}, \quad \nu = 0.2, \quad \gamma_C = 2500\,\text{kg/m}^3.$$

Properties of steel:

$$E_S = 200000\,\text{MPa}, \quad f_y = 450\,\text{MPa},$$
$$E_{ST} = 4000\,\text{MPa}, \quad \gamma_S = 7850\,\text{kg/m}^3.$$

Parameters of the La Borderie [1991] model:

$$\beta_1 = 1\,\text{MPa}, \quad \beta_2 = -10\,\text{MPa}, \quad y_{01} = 3.05 \times 10^{-4}\,\text{MPa},$$
$$y_{02} = 5 \times 10^{-3}\,\text{MPa}, \quad A_1 = 4.0 \times 10^3\,\text{MPa}^{-1}, \quad A_2 = 6.8\,\text{MPa}^{-1},$$
$$B_1 = 0.95, \quad B_2 = 0.7705, \quad \sigma_f = 2.6\,\text{MPa}.$$

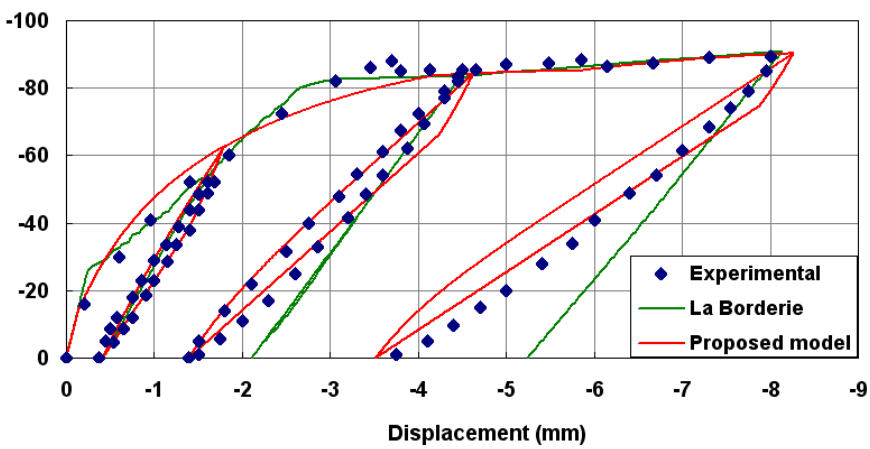

Figure 15. Load/displacement curve for beam in [Mazars et al. 2000].

Parameters of the simplified model under study:

$$M_{cr} = 5.04\,\text{kN·m}, \quad M_p = 26.1\,\text{kN·m}, \quad M_u = 28.35\,\text{kN·m},$$
$$\gamma = 6, \quad \phi_{pp} = 1.8 \times 10^{-3}\text{rad}, \quad \phi_{pu} = 7.0 \times 10^{-3}\text{rad},$$
$$X_\infty = 3.15\,\text{kN·m}, \quad b = 5000\,\text{kN·m}, \quad M_k = 0.0315\,\text{kN·m}.$$

The La Borderie [1991] model was used in the discretization process with 14 equal elements while for the simplified model, the structure was discretized in two equal elements.

A close observation of the curves in Figure 15 shows the La Borderie [1991] model satisfactorily reproduces the displacement curve. However this model is not capable of reproducing the two experimentally observed hysteresis curves. Moreover, the residual displacements are shown to be considerably distant from experimental results (in this model both plastifications of concrete and steel reinforcement are considered).

The displacement curve obtained from the simplified model under study is shown to be very realistic. Above all, it is worth emphasizing that this model is capable of reproducing hysteresis loops and also reproduces residual displacements with a remarkably high precision.

The second example explores the efficiency of the simplified model to reproduce the behavior of a structure submitted to loading with inversion of sign. The results of experimental and numerical analyses carried out for a frame presented by Alva [2004] are given. For this structure, the geometry and reinforcement distribution are shown in Figure 16.

In this test, the general loading procedure consisted of applying a constant point load of $F_N = 240\,\text{kN}$ in the column direction to simulate gravitational load, and of a variable load at the beam end to simulate

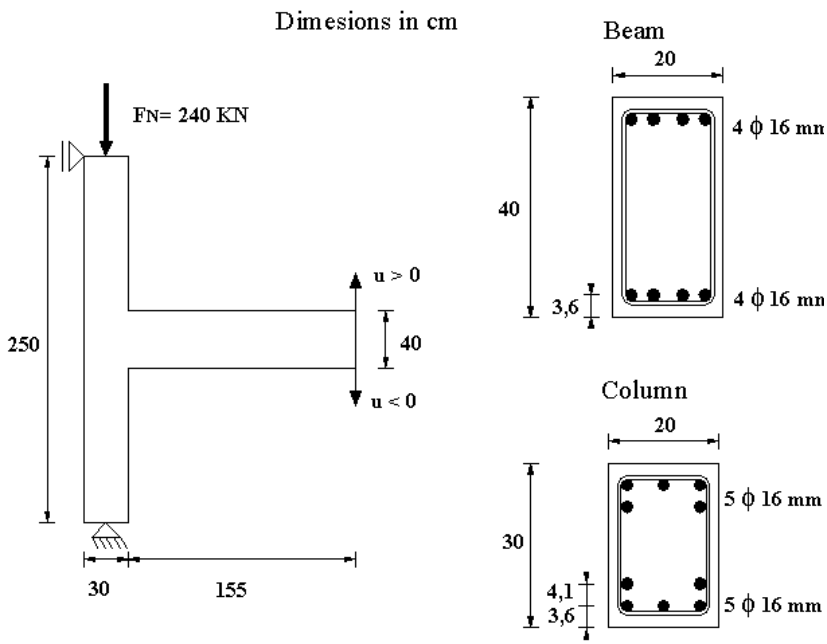

Figure 16. Frame subjected to load with sign inversion [Alva 2004].

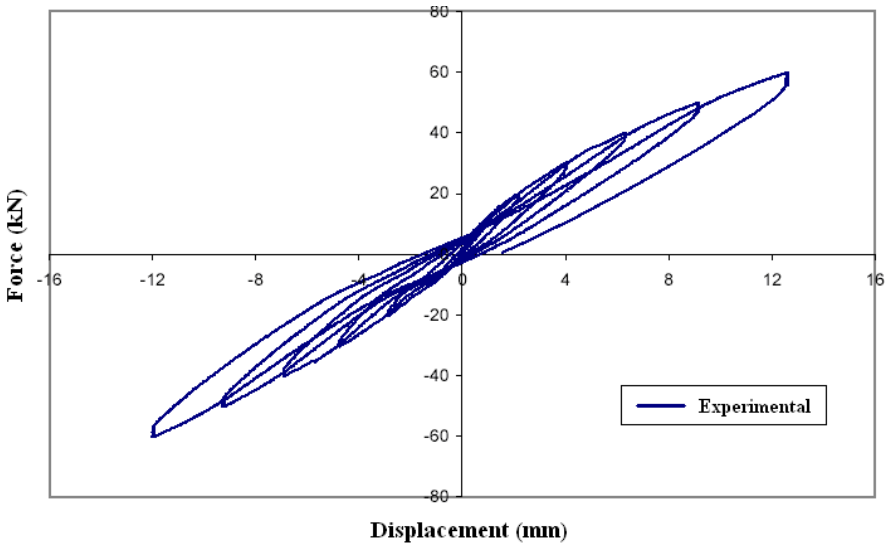

Figure 17. Beam end experimental load-displacement curve [Alva 2004].

cyclic load in multiple floor buildings [Alva 2004]. The sign convention for displacements measured at the beam end is indicated in Figure 16.

Figure 17 presents the experimental force-displacement response. The cyclic loading process at the beam end was initiated after the column normal load had been applied. The maximum and minimum applied loads were ±10 kN, ±20 kN, ±30 kN, ±40 kN, ±50 kN and ±60 kN, in totalizing six cycles.

The model in [La Borderie et al. 1991] and the simplified model under study are employed in simulating the numerical response. The material properties and the necessary parameters considered for application of these models are shown. For the model in [La Borderie et al. 1991], average concrete parameters are used while for the simplified model, the parameters employed were obtained from the results of [Alva 2004]:

Properties of the concrete:

$$E_C = 28315\,\text{MPa}, \qquad \nu = 0.2, \qquad \gamma_C = 2500\,\text{kg/m}^3.$$

Properties of steel:

$$E_S = 200000\,\text{MPa}, \qquad f_y = 600\,\text{MPa},$$
$$E_{ST} = 10500\,\text{MPa}, \qquad \gamma_S = 7850\,\text{kg/m}^3.$$

Parameters of the model in [La Borderie et al. 1991]:

$$\beta_1 = 0.8\,\text{MPa}, \qquad \beta_2 = -10\,\text{MPa}, \qquad y_{01} = 1.0 \times 10^{-4}\,\text{MPa},$$
$$y_{02} = 1 \times 10^{-3}\,\text{MPa}, \qquad A_1 = 8.0 \times 10^3\,\text{MPa}^{-1}, \qquad A_2 = 6.8\,\text{MPa}^{-1},$$
$$B_1 = 0.85, \qquad B_2 = 0.7705, \qquad \sigma_f = 2.6\,\text{MPa}.$$

The simplified model parameters for both $M > 0$ and $M < 0$ are:

Beam:

$$M_{cr} = 11.7\,\text{kN·m}, \quad M_p = 139.5\,\text{kN·m}, \quad M_u = 167.4\,\text{kN·m},$$
$$\gamma = 10, \quad \phi_{pp} = 2.5 \times 10^{-3}\text{rad}, \quad \phi_{pu} = 11.0 \times 10^{-3}\text{rad},$$
$$X_\infty = 18.6\,\text{kN·m}, \quad b = 7000\,\text{kN·m}, \quad M_k = 0.186\,\text{kN·m}.$$

Column:

$$M_{cr} = 17.1\,\text{kN·m}, \quad M_p = 117.9\,\text{kN·m}, \quad M_u = 130.5\,\text{kN·m},$$
$$\gamma = 5, \quad \phi_{pp} = 1.0 \times 10^{-3}\text{rad}, \quad \phi_{pu} = 4.0 \times 10^{-3}\text{rad},$$
$$X_\infty = 14.5\,\text{kN·m}, \quad b = 7000\,\text{kN·m}, \quad M_k = 0.145\,\text{kN·m}.$$

In the case of applying the model in [La Borderie et al. 1991], the structure was discretized in 9 elements: 4 column elements of equal length and 5 beam elements. In the case of the simplified model, only two column and one beam elements were considered.

Figure 18 presents the numerical response obtained from the model in [La Borderie et al. 1991]. The figure shows that although this model reproduces the plastic strain associated to the concrete, it underestimates the experimental residual displacement. It is worth observing also that the unloading path is described by practically straight line which is a little distant from the experimental curve.

Figure 19 presents the numerical response obtained from applying the model under study with hysteresis. As can be observed, the model satisfactorily reproduces the structural behavior and is capable of reproducing residual displacements associated to the plastic behavior of concrete, which are much closer to experimental results.

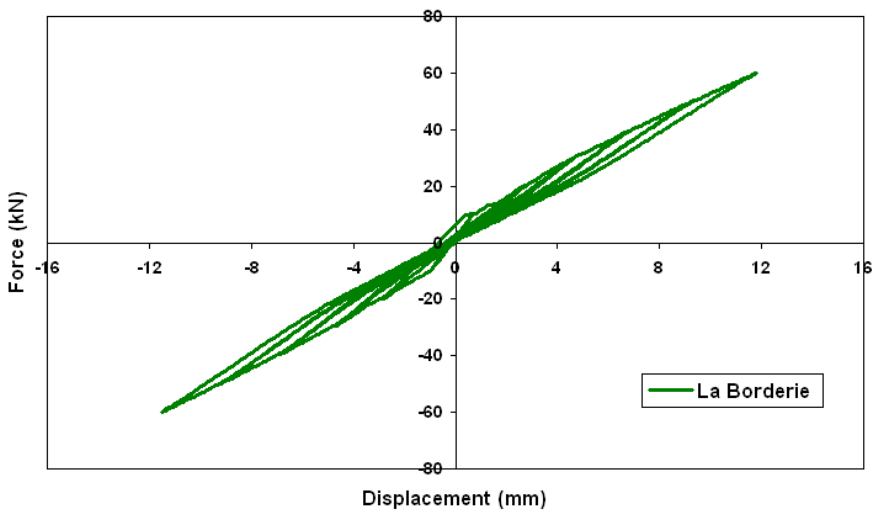

Figure 18. Beam end numerical load-displacement curve, the model in [La Borderie et al. 1991].

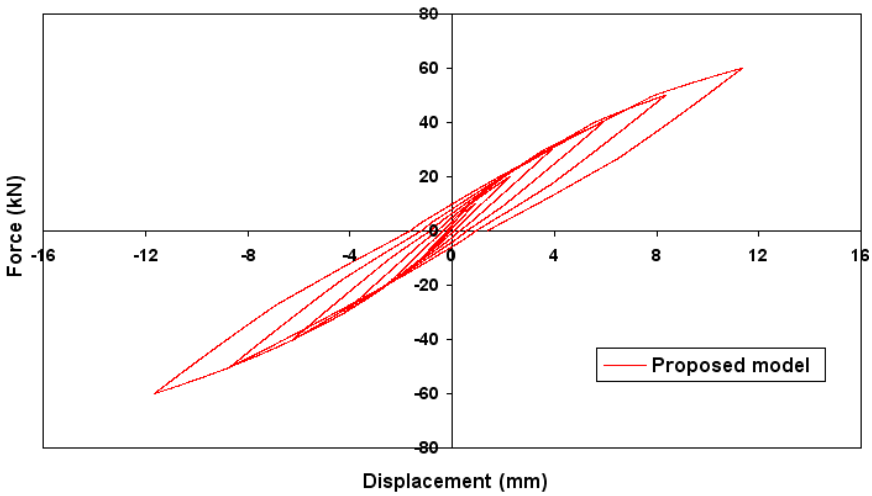

Figure 19. Beam end numerical load-displacement curve, proposed model.

7. Conclusions

The formulation of the simplified model is based on generalized variables that are consistent with the classical bending theory of bars. The parameters involved (cracking and plastification moments, and the corresponding kinematic parameters) can be obtained from conventional moment-rotation experimental procedures.

To evaluate the efficiency of the model, the results from the obtained model were compared with known experimental responses of reinforced concrete structures under load with the possibility of sign inversion. The numerically obtained force-displacement diagrams were shown to satisfactorily reproduce the experimental response. It was evidenced that the relative movement between the fracture surfaces in the concrete, particularly revealed during the unloading and reloading cycles, is important for any refined consideration of the effects of damage on structural behavior.

References

[Alva 2004] G. M. S. Alva, *Theoretical and experimental study of reinforced concrete frame joints behaviour under cyclic loads*, Doctoral Thesis, São Carlos School of Engineering. University of São Paulo. São Carlos, 2004. in portughese.

[Alves and Lubliner 1992] B. K. Alves and J. Lubliner, "A damage mechanics model for beams: Application to reinforced concrete beams", pp. 277–286 in *Numerical methods in engineering*, edited by H. Alder et al., Barcelona, 1992. Proc. CIMNE.

[Cohn and Franchi 1979] Z. M. Cohn and A. Franchi, "Strupl: A computer system for structural plasticity", *J. Struct. Div., ASCE* **105**:4 (1979), 789–804.

[Flórez-López 1993] J. Flórez-López, "Calcul simplifié de portiques endommageables", *Rev. Eur. Éléments Finis* **2**:1 (1993), 47–74.

[Flórez-López 1995] J. Flórez-López, "Simplified model of unilateral damage for RC frames", *J. Struct. Eng.* **121**:12 (1995), 1765–1772.

[Flórez-López 1998] J. Flórez-López, "Frame analysis and continuum damage mechanics", *Eur. J. Mech. A Solids* **17**:2 (1998), 269–283.

[Kachanov 1984] L. M. Kachanov, "On brittle fracture of a thin plastic interlayer in creep conditions", pp. 191–199 in *Mechanics of material behavior*, edited by G. Dvorak and R. Shield, Elsevier, Amsterdam, 1984.

[La Borderie 1991] C. La Borderie, *Phénomènes unilatéraux dans un matériau endommageable: modélisation et application à l'analyse de structure en béton*, Thèse doctorat, Université de Paris VI, Paris, 1991.

[La Borderie et al. 1991] C. La Borderie, G. Pijaudier-Cabot, and J. Mazars, "Response of plain and reinforced concrete structures under cyclic loadings", Rapport Interne 123, Laboratoire de Mécanique et Technologie, Cachan, France, 1991.

[Lemaitre and Chaboche 1974] J. Lemaitre and J. L. Chaboche, "A non-linear model of creep-fatigue damage cumulation and interation", in *Iutam symp. of mechanics of viscoelastic media and bodies*, Springer, Gothenburg, 1974.

[Lemaitre and Chaboche 1985] J. Lemaitre and J. C. Chaboche, *Mécanique de matériaux solides*, Dunod-Bordas, Paris, 1985.

[Maier et al. 1973] G. Maier, L. De Donato, and L. Corradi, "Inelastic analysis of reinforced concrete frames by quadratic programming", pp. 265–288 in *Symp. on inelasticity and nonlinearities in struct. concr.*, Univ. of Waterloo, Canada, 1973.

[Marigo 1985] J. J. Marigo, "Modeling of brittle and fatigue damage for elastic material by growth of microvoid", *Eng. Fract. Mech.* **21** (1985), 861.

[Mazars 1984] J. Mazars, *Application de la mécanique de l'endommagement au comportement non linéaire et à la rupture du béton de structure*, Thèse (Doctorat d'etat), Université Paris 6, Paris, 1984.

[Mazars et al. 2000] J. Mazars, F. Ragueneau, and G. Pijaudier-Cabot, "Continuum damage modelling for concrete structures in dynamic situations", pp. 259–294 in *Continuum damage mechanics of materials*, Damage mechanics of materials and structures, Cachan, France, 2000. Cachan, CNRS. 36p.(Lectures series), 2000.

[Mulas and Filippou 1990] M. G. Mulas and F. C. Filippou, "Analytical procedures in the study of seismic response of reinforced concrete frames", *Eng. Struct.* **12** (Jan. 1990), 37–48.

[Murakami 1981] S. Murakami, "Effects os cavity distribution in constitutive equations of creep and creep damage", in *Euromech colloque on damage mechanics*, Cachan, France, 1981.

[Ortiz and Simo 1986] M. Ortiz and J. C. Simo, "An analysis of a new class of integration algorithms for elastoplastic constitutive relations", *Int. J. Numer. Methods Eng.* **23** (1986), 353–366.

[Ragueneau et al. 2000] F. Ragueneau, C. La Borderie, and J. Mazars, "Damage model for concrete-like materials coupling cracking and friction, contribution towards structural damping: first uniaxial applications", *Mech. Cohes.-Frict. Mat.* **5** (2000), 607–625.

[Riva and Cohn 1990a] P. Riva and M. Z. Cohn, "Engineering approach to non-linear analysis of concrete structures", *J. Struct. Div., ASCE* **116**:8 (1990), 2162–2185.

[Riva and Cohn 1990b] P. Riva and M. Z. Cohn, "Engineering approach to non-linear analysis of concrete structures", *J. Struct. Div., ASCE* **116**:8 (1990), 2162–2185.

[Simo and Ju 1987] J. C. Simo and J. W. Ju, "Stress and strain based continuum damage models, I: Formulation", *Int. J. Solids Struct.* **23** (1987), 821.

[Tai 1990] W. H. Tai, "Plastic damage and ductile fracture in mild steels", *Eng. Fract. Mech.* **37** (1990), 853.

Received 19 Jan 2007. Accepted 30 Nov 2007.

FRANCISCO ADRIANO DE ARAÚJO: fco-adriano@bol.com.br
Escola de Engenharia de São Carlos, Departamento de Engenharia de Estruturas, Av. Trabalhador São-carlense, 400, 13566-590 São Carlos SP, Brazil

SERGIO PERSIVAL BARONCINI PROENÇA: persival@sc.usp.br
Escola de Engenharia de São Carlos, Departamento de Engenharia de Estruturas, Av. Trabalhador São-carlense, 400, 13566-590 São Carlos SP, Brazil
http://www.set.eesc.usp.br/public/pessoas/professor.php?id=23